Association of a KMT2D mutation with endocrine and hepatobiliary pathology: A case report

Petr Hotmar,[1*]

[1]Department of Chemical and Biomedical Engineering, Florida State University

[*]To whom correspondence should be addressed; E-mail: petr.hotmar@gmail.com

We report an unusual case of Kabuki syndrome associated with biliary atresia and endocrinopathies, and suggest a likely association of the causative mechanisms with the underlying KMT2D mutation. We discuss the pathologies in the context of laboratory, imaging, and modeling data, correlate latest findings of the relevant genetics studies, and outline the prospective therapies.

Background

The patient was diagnosed with a Kabuki syndrome (KS) based on typical dysmorphic features and the presence of a heterozygous pathogenic variant in a KMT2D gene. The penetrance for such variants appears complete, expressivity highly variable, prevalence outside Japan approximately 1:86000 (*1*). KS can be classified as a neurocristopathy (*2*).

Case Report

A female patient's prenatal ultrasound (US) indicated single umbilical artery (SUA), persistent left superior vena cava (PLSVC) and a solitary liver cyst; amniocentesis showed normal kary-

otype. She was born via Caesarean section in a breech position at a preterm gestational age of 33+6 weeks after a routine cardiotocography (CTG) exam indicated placental insufficiency and fetal distress (meconium in amniotic fluid, APGAR score 7-8-9), with the birth weight of 1710 g and head circumference of 27.5 cm. There was no consanguinity between parents, with unremarkable family history and no history of genetic disorders. The postnatal electrocardiogram showed patent foramen ovale (PFO) and right ventricular hypetrophy (RVH), with no coarctation, abdominal x-ray (AXR) indicated meconium ileus. Bloodwork revealed neonatal hypoglycemia, jaundice and antithrombin (AT) deficiency. Double-barrel jejunostomy was performed to resolve microcolon. The following month the patient exhibited frequent hypoglycemia, (need of up to 20 g glucose/kg/day to maintain euglycemia), hypotension (treated with fresh frozen plasma (FFP) and dopamine), anemia (transfusion (TRF) of packed red blood cells (PRBC)), coagulopathy (TRF of FFP) and a necrotizing enterocolitis (NEC) episode preceded by metabolic and respiratory acidosis (treated conservatively with mechanical ventilation, antibiotics (ATB) – Meronem and Metrondiazole, later Targocid and Fluconazol – and TRF of FFP and PRBC). She was diagnosed with congential hypothyroidism (no involvement of hypothalamus-pituitary axis, FT4 4.37 pmol/l, TSH $>$150 mIU/l) and started on levothyroxine therapy (LT), later increased to 22 μg/day/kg of body weight to maintain euthyroid.

Susp. cholangitis was treated with Sulperazone, endoscopic retrograde cholangiopancreatography (ERCP) revealed extrahepatic biliary atresia (BA) (confirming communication between the hepatic cyst and gall-bladder, with the contrast agent not entering duodenum). The cyst was marsupialized and an external T-tube advanced to the gallbladder to drain the serous transudate (lactate dehydrogenase 0.8 μkat/l, triglycerides 0.06 mmol/l, cholesterol 0.31 mmol/l, total protein 0.23 g/l). Liver biopsy, with a sample obtained by wedge excision, revealed diffuse intracelluar and canallicular cholestasis with disperse inflammation in portal canals. Due to the heterogeneous nature of the pathology combined with high sampling error, the sample was not

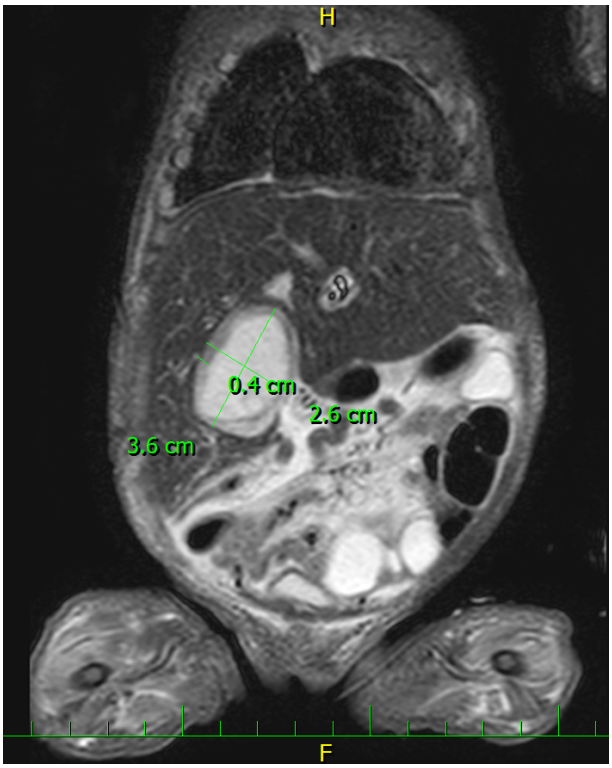

Figure 1: MRCP at one month of age: A liver cyst of approx. 3.6×2.6 cm, with a 0.4 cm thick wall. Acquisition parameters: 1.5T magnet, STIR, TR=1660 ms, TE=70 ms, slice thickness 4 mm.

sufficiently representative to make further determinations. Magnetic resonance cholangiopancreatography (MRCP) confirmed a thick-walled cyst at the left/right lobe interface, see Fig. 1, and hepatomegaly with left lobe distended and displaying occasional dilation of bile ducts, see Fig 2.

At 2 months of age, a chronic catheter-related sepsis of a 2-month duration, with concomittant hepatosplenomegaly and a rise in levels of acute-phase proteins, developed due to iliofemoral deep vein thrombosis (DVT) and thrombophlebitis, and was treated with low-molecular-weight heparin (LMWH) and Clexane, TRF (FFP, PRBC, platelets (PLT)), mechanical ventilation and ATB therapy – Klebsiella pneumoniae in blood culture (BC) and on cathether tip (ATB Tazocin, Gentamicin, Fluconazole), Citrobacter ESBL in BC (ATB Amikacin, Imipenem, Flu-

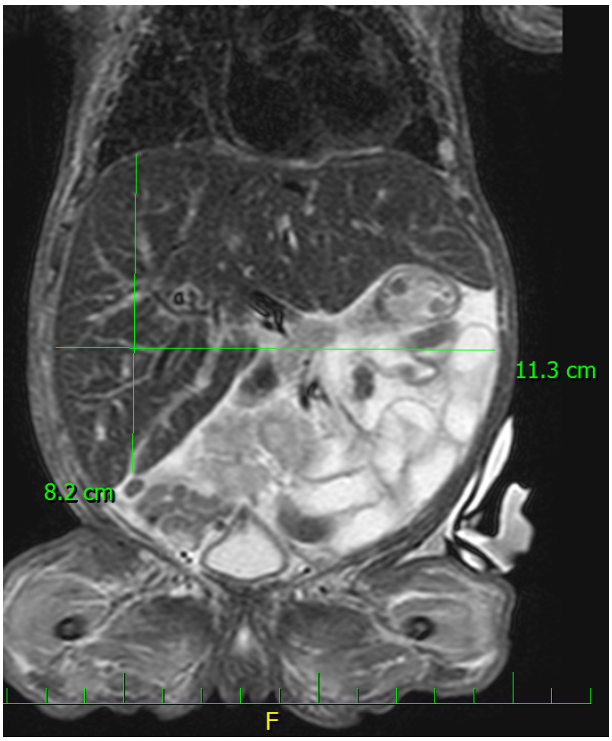

Figure 2: MRCP at one month of age: Hepatomegaly with a distended left lobe, and apparent intra-hepatic and intra-abdominal fluid. Acquisition parameters: 1.5T magnet, STIR, TR=1660 ms, TE=70 ms, slice thickness 4 mm.

conazole), Candida glabrata (Capsofungin), Staf. epidermis (Biseptol, Kolomycin).

Hypotonia, underdeveloped newborn reflexes, microcephaly, mild hypertelorism and strabismus, micrognathia, and low-set ears (with one dysplastic) suggested a possible genetic disorder, later diagnosed as KS (chromosomal microarray analysis indicated a de novo mutation in a Kabuki gene KMT2D, c.16294C>T, classified as likely pathogenic, and a likely benign variant c.8552G>A, found also in a healthy father). In addition, two heterozygous variants of unknown significance (VUS) were identified, namely in the gene CHD7 (c.164C>T) and PDGFRB (c.164C>T). Whole-genome array CGH did not reveal any abnormalities. Metabolic screening revealed mild biotinidase deficiency and iminoglycinuria.

The juejunostomy was successfully reversed 4 months after placement, with enteral nutrition, by naso-gastric tube due to dysphagia, started and well-tolerated (initially breast milk, after hematochezia and GGT spike at 18 ukat/l, with susp. milk allergy, switched to Neocate and Fantomalt). The gall-bladder drain tube tested repeatedly positive for colonization (Stenotrophomonas, susp. cholangitis treated with Sulperazone, later Sumetrolim).

At 5 months of age, brain MRI showed minor signal alteration in cortical and juxta-cortical white matter (WM) (parietal-occipital, dorsally, right), likely post-hypoxemic, slightly delayed WM myelination, corpus callosum hypoplasia, borderline antero-posterior diameter of foramen magnum (0.8 cm), and diminished posterior pituitary hyperintensity, see sagittal and axial images in Figs. 3, 4, 5. Chest x-ray showed stationary cardiomegaly and thymus hyperplasia, see Fig. 6, abdominal and pelvic US confirmed persistent hepatosplenomegaly and diffuse lesions with periportal fibrosis. Brainstem auditory evoked potential (BAEP) showed increased latency for right ear waves III and V with left ear normal, flash electroretinogram (f-ERG) and flash visual evoked potentials (f-VEP) also normal.

At 6 months of age the liver transplant was deemed contra-indicated due to corpus callosum hypoplasia, bronchopulmonary dysplasia, ren arcuatus, microcephaly, and intestinal malabsorp-

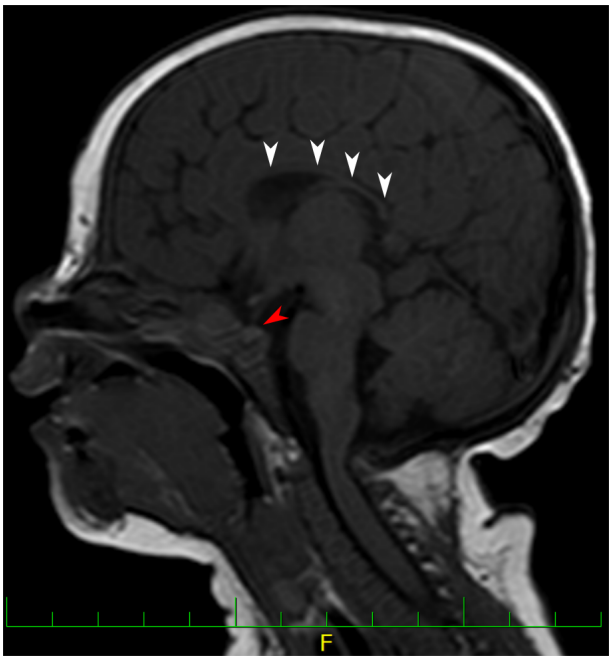

Figure 3: Midline sagittal T1-weighted (spin echo) image, chronological age 5 months, shows diffusely thin corpus callosum (CC, white arrows) with absence of rostrum and genu, likely due to secondary destruction (considering development from anterior to posterior aspect). However, given a slower growth of CC in premature infants, the appearance is time-dependent. Note also the diminished vasopressin-associated hyperintensity of the posterior pituitary lobe (red arrow), possibly related to GHD (*3*).

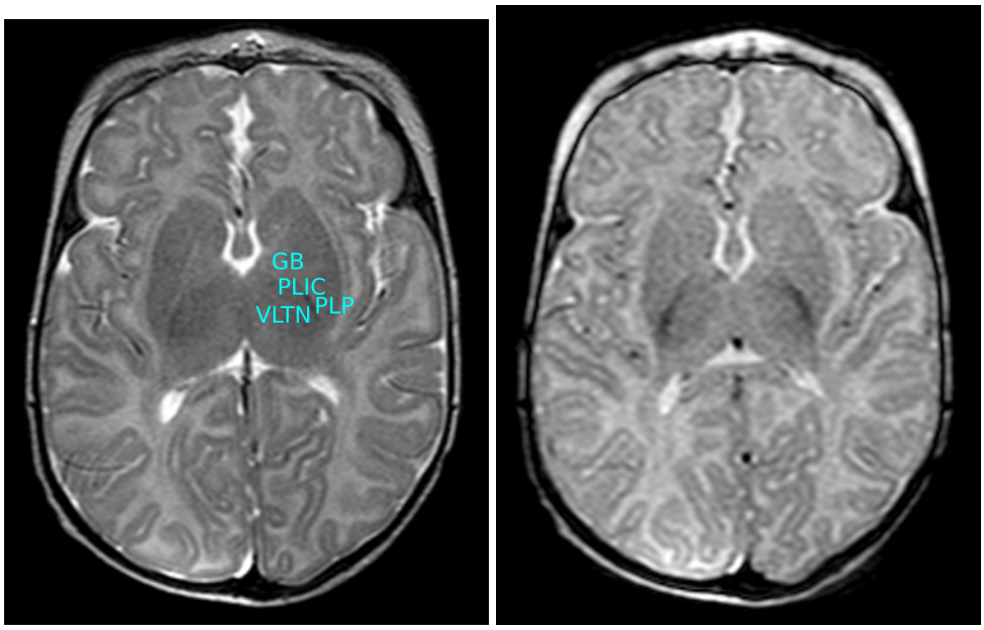

Figure 4: Axial T2-weighted (turbo spin echo, left) and T1-weighted (inversion recovery, right) images show slightly delayed myelination and some indications of hypoxic-schemic injury. The PLIC are well visualized and more hypointense than PLP, with some hypointensity also appreciated in VLTN – these hypointense landmarks are typically lost in HIE of basal ganglia (*4*). On the other hand, fairly hyperintense GB, especially relative to PLP, suggests some degree of HIE, possibly due to sepsis-associated hypoxia and bilirubin encephalopathy (between the 3rd and 5th months of age the unjconjugated bilirubin in serum repeatedly reached around 50 μmol/l).

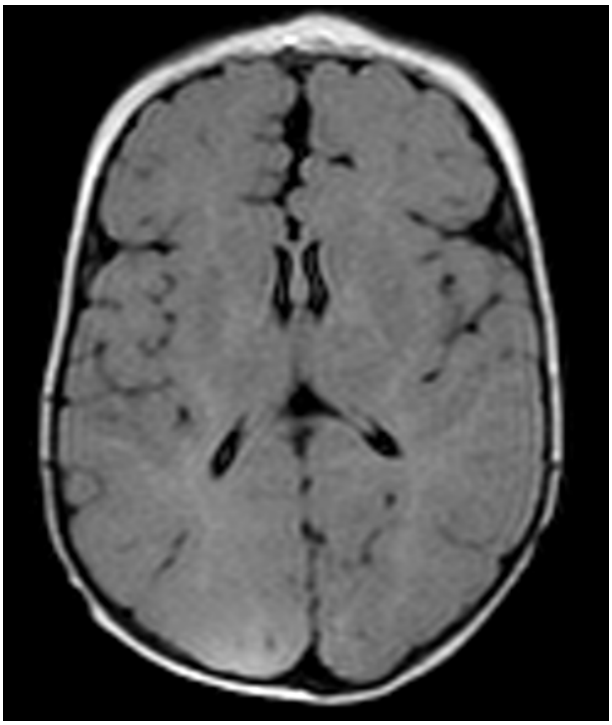

Figure 5: Axial FLAIR (fluid-attenuated inversion recovery) image shows hyperinstense lesions in in cortical and subcortical white matter in right occipital lobe.

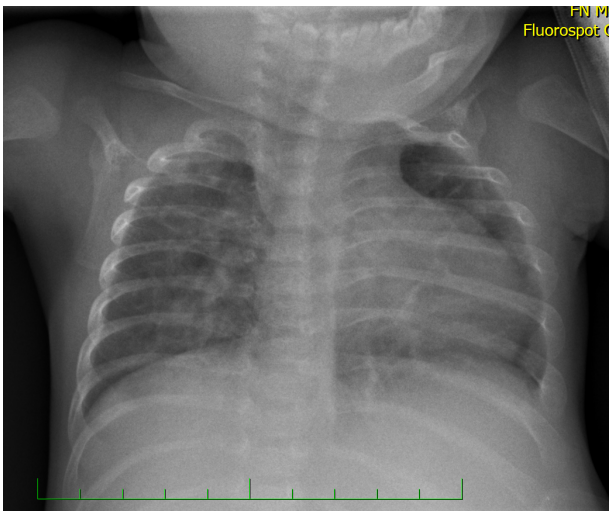

Figure 6: Chest X-ray at 5 months of age showing cardiomegaly and thymus hyperplasia. Note also malocclusion in mandible, possibly associated with deficient expression of KMT2D, as discussed below.

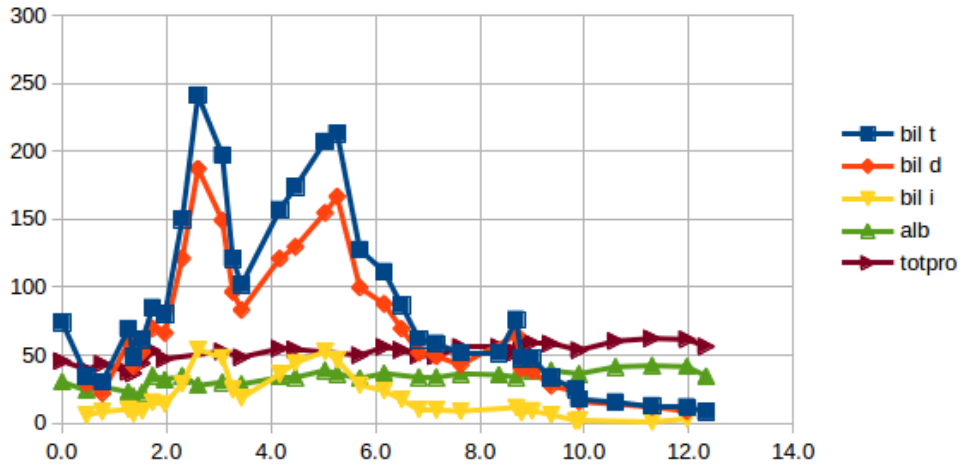

Figure 7: Time evolution of liver function. X-axis = chronological age in months. Y-axis: plasma concentrations of bilirubin total, direct and indirect [umol/l], albumin and total protein [g/l].

tion. The patient was discharged into home care, with subsequent 6 months rather uneventful (peripherally inserted central catheter (PICC) malposition treated with removal and insertion of a tunneled Broviac central venous catheter (CVC) via v. subclavian l. dx., mild episode of enterocolitis and upper respiratory infection were both treated conservatively). Liver function (BIL, ALB, TOTPRO) and liver enzymes (except for GGT) returned to a reference range, see Figs. 7 and 8, likely due to external biliary drainage (approx. 200 ml of biliary transudate per day, with hepatic cyst size regression from its maximum at 120 ml during tube blockage to below 20 ml). Over the 6 months of LT the thyroid function stabilized, with FT4 increase from initial 4 to 18 pmol/l, and TSH decrease from initial 150 to 4 mIU/l.

At 9 months of age the gallbladder tube malposition and blockage prompted creation of a new fistula and placement of a 12F pigtail catheter into the cystoid, see Fig. 9. An MRCP showed occasional dilation of intrahepatic bile ducts (width up to 4 mm) in both lobes, with diffuse leakage likely due to chronic inflammation, and chronic splenomegaly, see Fig. 10

At 10 months of age, after a 3-month stagnation of body weight, the partial parenteral nutri-

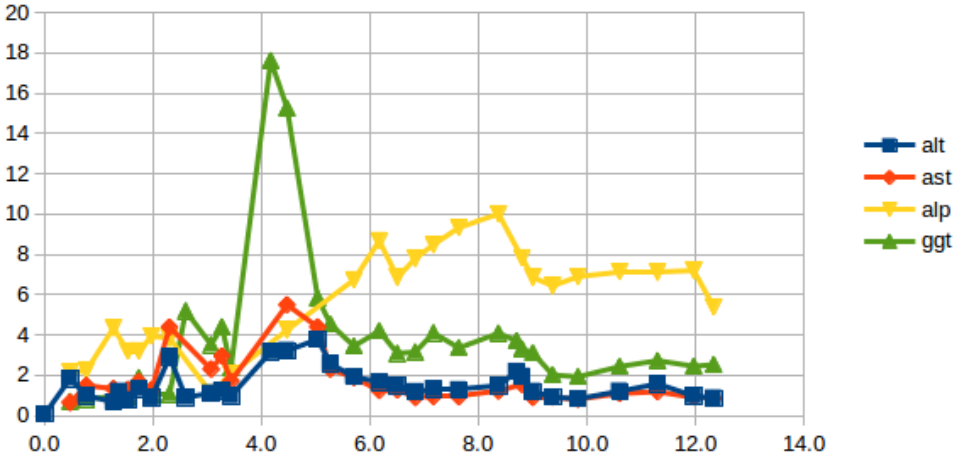

Figure 8: Time evolution of liver enzyme levels. X-axis = chronological age in months. Y-axis: plasma concentrations of ALT, AST, ALP, GGT [ukat/l].

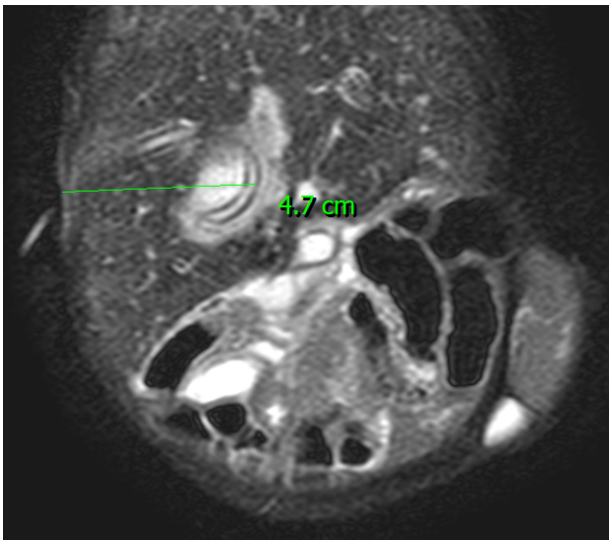

Figure 9: MRCP at 9 months of age: Catheter draining biliary transudate from the liver cystoid. Note diffuse dilation and leakage of intrahepatic bile ducts. Acquisition parameters: 1.5T magnet, STIR, TR=1797 ms, TE=70 ms, slice thickness 4 mm.

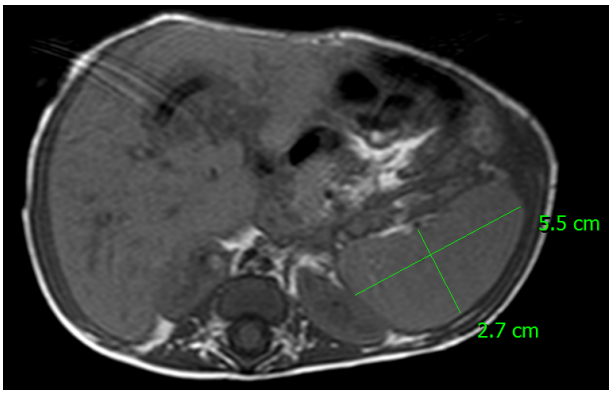

Figure 10: MRCP at 9 months of age, transverse section: Chronic splenomegaly (size variable, up to 7 cm), possibly due to portal hypertension and chronic inflammation. Acquisition parameters: 1.5T magnet, T1-TSE, TR=600.5 ms, TE=17 ms, slice thickness 4 mm.

tion, consisting of 10% glucose, amino acid solution and electrolytes to compensate for hepatic drain losses, was supplemented with a lipid emulsion. An isolated mammary gland enlargement, likely indicative of premature thelarche, was confirmed by neck US, with serum levels of gonadotropins in reference range (RR), IGF1 at 19 μg/l (RR 125+-93) and IGFBP3 at 1 mg/l (RR 6.7+-2.1). The causes of recurrent hypoglycemia (down to 2.5 mmol/l) and decreased levels of IGF-1 and IGFBP-3 are currently being investigated.

Discussion

Endocrinopathies: Congenital Hypothyroidism, Persistent Hypoglycemia and Premature Thelarche

Missense variants in the terminal regions of KMT2D are speculated to increase the risk for autoimmune disease (*1*). While serum levels of antithyroid antibodies have not been evaluated in the patient, the diagnosis of autoimmune thyroiditis might be supported by laboratory findings (high TSH and low FT4 levels, both normalized after LT) and neck US (hypoechogenic thyroid with volume reduction from 2.1 ml to less than 1 ml after a year of LT, see Fig. 11). Alternatively, as KMT2D demonstrates expression in thyroid, a dysmorphogenesis due to compromised

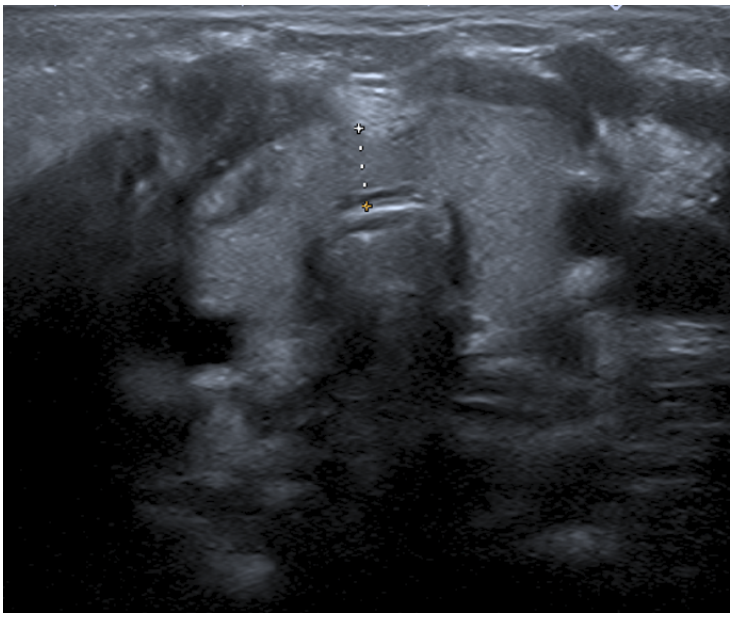

Figure 11: Thyroid at 5 months of age, volumes of left and right lobes 1 and 0.8 ml, respectively, isthmus 4.2 mm.

thyroid hormone biosynthesis (including transporters, enzymes or thyroglobulin) offers another potential causality, though the underlying mechanism is unclear (*5*). Both endocrine disorders (hypothyroidism, premature thelarche) can be expected to resolve with time (*1, 6*).

While the cause for persistent hypoglycemia remain unknown (see the Appendix for details on a computational model of glucose dynamics), possible causal candidates could include GHD and/or KMT2D-induced effects on SLC2A3 glucose transporter. Other Kabuki-related causes reported in literature include hyperinsulinism and ACTH deficiency (*7*). Thus, GHD and hypothalamo-hypophyseal dysfunction need be considered in differential diagnosis, especially since these have been described in patients with the same missense mutation (*8*). The diminished bright spot at posterior pituitary in the T1-weighted MRI, Fig. 3, and the low levels of IGF-1 and IGFBP-3 lend further credence the GHD hypothesis (*3*). Another patient with the same mutation, shown to disrupt a secondary active site in the COMPASS complex, exhibited autoimmune diseases associated with humoral immune deficiency, possibly due to KMT2D

binding multiple cofactors critical for B-cell terminal differentiation (PAX transcription activation domain interacting protein, PTIP) (*9*). Other immune deficiencies, incl. recurrent otitis media, are also commonly described in KS patients.

GIT Disorders: Biliary Atresia and Intestinal Malabsorption

With the pediatric liver transplant (PELT) offering the only long-term treatment to BA, intestinal malabsorption (IM) constitutes here the only absolute contra-indication to the PELT due to a potential compromise of immunosuppressive therapy. What is the underlying pathophysiology of IM? Ruling out inadequate transit time (rate of fecal evacuation normal), disturbed gastric motility/secretion (no indication thereof, normal serum levels of vitamin B12, iron, calcium and magnesium), and pancreatic exocrine insufficiency (no indication thereof, serum levels of alpha-amylase and lipase normal), we focus on small intestine malabsorption. As the quantitative loss of absorptive intestinal surface during jejunostomy-associated resection was minimal, we do not consider a short bowel syndrome to be a major contributor to the IM; this hypothesis is further supported by adequate serum levels of trace elements (particularly zinc and selenium), calcium, magnesium, iron and folic acid (*10*). The most likely cause thus remains the absence of biliary secretion in duodenum, with the resulting interruption of enterohepatic circulation and compromise of lipid digestion, as evidenced clinically by steatorrhea and deficiencies in fat-soluble vitamins. Further external drainage-related causes likely include loss of nutrients through the drain, and intestinal dismicrobia due to a) cholestasis-induced lipid malabsorption, and b) chronic ATB therapy aimed at controlling bacterial colonization of the drain (intra- and extra-luminal). Potential co-contributors to IM include an undiagnosed and/or KMT2D-related deficiency in enteral mucosa enzymes or carrier mechanisms.

Molecular Genetics and Prospective Therapies

The observed missense mutation c.16294C>T in KMT2D gene results in the amino acid change p.R5432W in exon 51 in KMT2D, chromosomal location chr12:49416417. In this case KS is caused by haploinsufficiency for KMT2D gene that promotes the opening of chromatin. KMT2D is a histone 3 lysine 4 (H3K4) N-methyltransferase that modifies lysine at the fourth amino acid position of the histone H3 protein, catalyzing mono-, di- and tri-methylation of H3K4. As KMT2D functions as a regulator of chromatin expression, agents that promote chromatic opening, especially histone deacetylase inhibitors (HDACI)s, have been hypothesized to have beneficial effects, both exogenous and endogenous.

The KMT2D-encoded protein contains a highly conserved SET domain, and is part of the ASCOM protein complex, whose functions include the removal of repressive, and deposition of activating, epigenetic marks on chromatin, resulting in an activated (transcription-active) chromatin state. Defective KMT2D leads to imbalances in histone marks on downstream target genes, thereby compromising gene activation and suppression and resulting in errors in differentiation during embryonic development (*11*). As an enhancer regulator it functions not only in development and differentiation, but also in metabolism and tumor suppression (*12*). Incidentally, it has been shown (*13*) in a mouse model of KS that the introduction of a heterozygous KMT2D mutation in the SET domain correlates with abnormalities in the granule cell layer of the dentate gyrus, and with the associated hippocampal memory defects. Oral administration of HDACI led to normalization of both structural and functional deficits in the gyrus, suggesting that a reversible deficiency in postnatal neurogenesis may underlie intellectual disability in KS. As the neurogenesis potential is age-restricted a window-of-opportunity may exist for treatment, though it is unclear if the beneficial effects can be sustained long-term. Drugs with high potency, specificity and tolerance are being investigated, including exogenous HDACI (high potency, low specificity) or beta-hydroxybutarate, an endogenous HDACI transported during

ketosis (e.g. while on a ketogenic diet) into hippocampus (high specificity, low potency) (*14*).

KMT2D also plays role in regulating HOX genes (regulate axial patterning of the developing embryo) and embryonic growth. HOXC6 is critical for mammary gland development and regulation of bone morphogenic protein 7, fibroblast growth factor receptor 2 (FGFR2) and IGFBP3 (*6*). A knockout of KMT2D can downregulate HOXC6, modifying expression of FGFR2 and IGFBP3, and resulting in musculo-skeletal anomalies. Further, low hypothalamic sensitivity to suppressive effects of sex hormones on gonadotropin secretion could explain the premature thelarche like presented by the patient.

Expression of KMT2D was observed in dental epithelium of primary incisors, canine and molars, frequently leading to oro-dental abnormalities (*8*). The patient's chest x-ray shows malocclusion in mandible, to be further confirmed.

Conclusions

Acknowledgements

The author thanks the employees of the Motol University Hospital in Prague, Czech Republic, for helpful assessments, comments, and provision of data and information on which this case report heavily relies.

Appendix

Glucose Dynamics

At one year of age about 20 measurements of blood glucose were collected at specific times over 48 hours in an effort to investigate the cause of recurrent hypoglycemia. During this time, the patient was repeatedly on and off both enteral and parenteral nutrition so as to quantify the effects of both on the time evolution of the plasma glucose concentration. We used a single-

compartment kinetic model (*15*) to analyze some of the data. Given a body weight of 4.8 kg, infusion rate R_0 of 16 ml/min (with initial and final rates set to 6 ml/min to decrease the temporal gradient) and baseline glucose concentration c_0 of 3.1 mmol/l (obtained more than 4 hours after infusion stopped and more than 2 hours after last meal, thus assuming a fasting state), the model yields the clearance rate C_L of 30 ml/min/kg of body weight, distribution volume V_D of 5 l/kg of body weight, and the half-life $\tau_{1/2}$ of 112 min (all values are approximate). The 1st-order rate constant k for the attainment of steady state coincides with that for the elimination of glucose, and can be written as

$$k = \frac{V_D}{C_L} \approx 6 \times 10^{-3} \text{ min}^{-1}. \tag{1}$$

The model allows to compute the infusion rate R_r required to achieve the desired plasma concentration c_r after a given time t_r. E.g. for steady state concentration $c_r = c_{ss}$ and $t_r = 10$ min we obtain $R_r = 4.4$ ml/min, and about 19 g of glucose is needed to achieve this state.

The model assumes achievement of steady state concentration $c_{ss} \approx 4.7$ mmol/l after 7 hours of infusion, and inherently neglects other compartments, including endogenous glucose production.

The glucose dynamics over the course of a representative time window (including start-up and cessation of infusion, and enteral feeds) is shown in Fig. 12. We see two transient hypoglycemic states, one coinciding with the cessation of the infusion, the other following postprandial insulin spike. Hyperglycemia can be observed when enteral and parenteral feeds combine. The low fasting baseline (near the lower limit of the reference range) suggest dysregulation of glucose homeostasis due to deficient liver glycogenolysis and/or gluconeogenesis, with the potential causes discussed above.

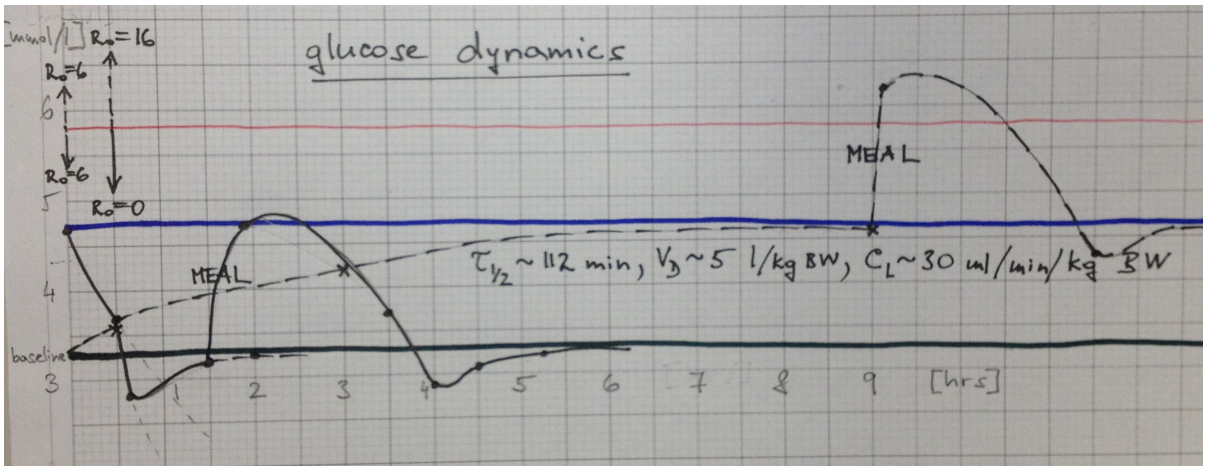

Figure 12: Glucose dynamics over a representative time period. The dashed line denotes start of infusion (analyzed by one-compartment kinetic model) with a subsequent meal, the solid line shows cessation of infusion with a subsequent meal. Black and red lines denote, respectively, the lower and upper limits of the reference range for blood glucose in the patient. The fasting baseline (approx. 3.1 mmol/l) is drawn to coincide with the lower limit of the reference range, the blue line denotes the infusion steady-state concentration. The black dots indicate the measurements, the interpolating curves are approximate.

About the author

Petr Hotmar received Master of Science in Cybernetics from The Institute of Chemical Technology, Prague, Czech Republic, Master of Science and Ph.D. in Chemical and Biomedical Engineering from Florida State University, Tallahassee, USA, and a post-doctoral fellowship in Plasma Physics from LAPLACE Laboratory in Toulouse, France. He specializes in computational physics, applied mathematics and biology.

References and Notes

1. M. P. Adam, L. Hudgins, M. Hannibal, *GeneReviews®*, M. P. Adam, *et al.*, eds. (University of Washington, Seattle).

2. K. B. Shpargel, J. Starmer, C. Wang, K. Ge, T. Magnuson **114**, E9046.

3. S. L. Tsai, E. Laffan **9**, 136.

4. A. P. Tan **1**.

5. C. Peters, A. S. P. van Trotsenburg, N. Schoenmakers **179**, R297.

6. J.-E. Moon, S.-J. Lee, C. W. Ko **19**, 102.

7. Y. A. Zarate, H. Zhan, J. R. Jones **3**, 180.

8. T. Porntaveetus, *et al.* **14**, 381.

9. A. W. Lindsley, *et al.* **137**, 179.

10. J. Keller, P. Layer **30**, 150.

11. E. Aref-Eshghi, *et al.* **12**, 923.

12. E. Froimchuk, Y. Jang, K. Ge **627**, 337.

13. H. T. Bjornsson, *et al.* **6**, 256ra135.

14. J. S. Benjamin, *et al.* **114**, 125.

15. R. G. Hahn **5**.

Acronyms

AT antithrombin. 2

ATB antibiotics. 2, 3, 10

AXR abdominal x-ray. 2

BA biliary atresia. 2, 9

BAEP Brainstem auditory evoked potential. 3

BC blood culture. 3

CTG cardiotocography. 1

CVC central venous catheter. 4

DVT deep vein thrombosis. 2

ERCP endoscopic retrograde cholangiopancreatography. 2

f-ERG flash electroretinogram. 3

f-VEP flash visual evoked potentials. 3

FFP fresh frozen plasma. 2, 3

GB globus pallidi. 5

GHD growth hormone deficiency. 4, 9

HDACI histone deacetylase inhibitors. 10, 11

HIE hypoxic ischemic encephalopathy. 5

IM intestinal malabsorption. 9, 10

KS Kabuki syndrome. 1, 3, 9–11

LMWH low-molecular-weight heparin. 2

LT levothyroxine therapy. 2, 6

MRCP Magnetic resonance cholangiopancreatography. 2

NEC necrotizing enterocolitis. 2

PELT pediatric liver transplant. 9

PFO patent foramen ovale. 2

PICC peripherally inserted central catheter. 4

PLIC posterior limbs of internal capsules. 5

PLP posterolateral putamen. 5

PLSVC persistent left superior vena cava. 1

PLT platelets. 3

PRBC packed red blood cells. 2, 3

RR reference range. 6

RVH right ventricular hypetrophy. 2

SUA single umbilical artery. 1

TRF transfusion. 2, 3

US ultrasound. 1, 6, 8

VLTN ventrolateral thalamic nuclei. 5

WM white matter. 3